Electrically induced deformation in chiral smectic elastomers with different domain structures

Yang Ho Na,[1,*] Yuki Aburaya,[2] Hiroshi Orihara,[2] Kazuyuki Hiraoka,[3] and Youngbae Han[4]

[1]*Department of Advanced Materials, Hannam University, Jeonmin-dong 461-6, Yuseong-gu, Daejeon 305-811, Korea*

[2]*Division of Applied Physics, Faculty of Engineering, Hokkaido University, North 13 West 8, Kita-ku, Sapporo 060-8628, Japan*

[3]*Department of Life Science & Sustainable Chemistry, Tokyo Polytechnic University, 1583 Iiyama, Atsugi 243-0297, Japan*

[4]*Department of Mechanical and Design Engineering, Hongik University, Sejong-ro 2639, Jochiwon-eup, Sejong 339-701, Korea*

(Received 29 August 2014; published 29 December 2014)

Electrical actuation is investigated in two kinds of chiral smectic liquid-crystal elastomers (LCEs) with different domain structures LCE1 and LCE2: The latter is better than the former in orientational order. Tracking fluorescent beads dispersed on the samples enables us to measure the two-dimensional strain tensors in ferroelectric elastomer films. It turns out that the electric-field-induced strain is polarity dependent and the type of molecular orientation responsible for the strain is specified. In LCE1 the shear strain is dominant, whereas in LCE2 it is comparable to the elongation strain, which is explained by the rotation of the principal axes. The essential differences of the two elastomers are observed in the eigenvalues of the strain tensors. The absolute values for LCE1 are larger than those for LCE2. The difference is discussed on the basis of the domain structures.

DOI: 10.1103/PhysRevE.90.062507 PACS number(s): 61.30.−v, 61.41.+e, 77.65.−j

I. INTRODUCTION

Liquid-crystal elastomers (LCEs) are unique materials that combine the anisotropy of liquid crystals with the elasticity of polymer networks [1,2]. Because of electromechanical and electro-optical properties, they have been paid increasing attention in the past two decades [3–11]. In particular, chiral smectic elastomers have attracted interest because of properties such as piezoelectricity, ferroelectricity, pyroelectricity, and second-harmonic generation [9–27]. Among them, piezoelectricity may be important in applications.

Deformation of a LCE by electric excitation is coupled with changes in the orientation of the director. For the orientational changes in chiral smectic phases, they represent modes like the soft mode in the smectic-A^* (Sm-A^*) phase (the condensation of which induces the Sm-A^*−Sm-C^* phase transition) and amplitude and phase modes in the Sm-C^* phase. If chiral smectic LCEs thus deform according to the modes that are excited by an electric field, the shear deformation should be observed in the chiral smectic LCEs as shown in previous studies [9–12]. We have recently succeeded in directly observing the electrically induced shear deformation in the Sm-C^* phase using a fluorescent bead-tracking method [26,27]. Previous studies only reported the piezoelectric property of the elongation strain along the film thickness direction (piezoelectric coefficient d_{xxx} in our coordinate system shown in Fig. 1) [9,10,22–25], whereas our study has shown the direct evidence of the piezoelectric property for electrically induced shear deformation (piezoelectric coefficient d_{xyz}) [26]. From the temperature dependence of strain tensors, we also found that the shear deformation was dominant and the origin of the shear strain was mainly attributed to the phase mode (the Goldstone mode) in the Sm-C^* phase [26]. The LCE used in the previous study is a uniaxially deformed elastomer (LCE1) [26,27]. As shown in Fig. 1 (left), the directors are uniformly aligned along the z axis, but are tilted with respect to the layer normal in the Sm-C^* phase of this elastomer [28]. The layer normals are conically distributed around the director. Layer tilting may thus cause domain boundaries to form in the Sm-C^* LCE. On the other hand, there is another elastomer with different domain structure (LCE2). In the Sm-C^* phase, it has a uniform structure in terms of the director and layer orientation shown in Fig. 1 (right) [28].

Some studies have already been reported on the piezoelectric effect in these elastomers [19,22,24,25]. Kremer and co-workers studied the direct and inverse piezoelectric effects d_{xxx} in the LCE2 sample [19,22,24]. Hiraoka *et al.* carried out the dynamic electromechanical measurements of the complex piezoelectric constant in LCE1 and LCE2 [25]. It was reported that a relaxation of the piezoelectric constant on frequency took place in LCE1, but the resonance in LCE2 and the piezoelectric constant of LCE2 with a macroscopically spontaneous polarization were smaller than those of LCE1 possessing no net spontaneous polarization.

The previous studies, however, measured no quantities directly related to the electrically induced shear deformation, which was essential in the chiral smectic elastomers. In this paper we measure the two-dimensional strain tensors in the deformation plane as a function of temperature for both LCEs to elucidate the effect of domain structure on piezoelectricity. After the experimental setup and analytical method are briefly described, the results of our experiments are presented and discussed. We then provide a summary of the work.

II. EXPERIMENT AND ANALYSIS

The ferroelectric LCEs prepared in this study were network polymers with two different liquid-crystal subunits attached comblike to a polysiloxane backbone. Chemical structures and molar ratios of molecular components were described in detail in a previous study [12]. Elastomers were synthesized by the hydrosilylation reaction of the side groups and the backbone according to the procedure previously reported by Finkelmann *et al.* [29]. The elastomer film was prepared by spin casting using a solution containing polysiloxane, two mesogens, a cross-linker, and a Pt catalyst in toluene. The reaction was

*Author to whom correspondence should be addressed: yhna@hnu.kr

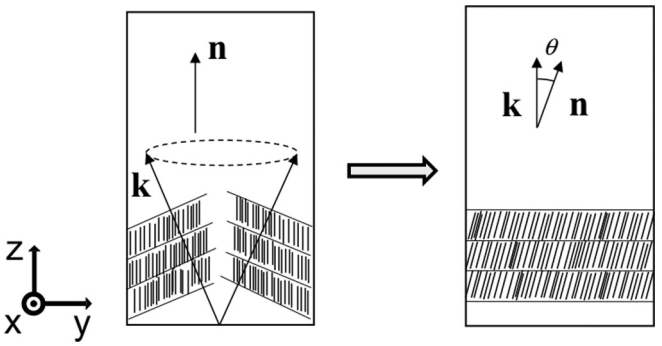

FIG. 1. Schematic of the molecular alignment in LCE1 (left) and LCE2 (right) in the Sm-C^* phase. Here **n**, **k**, and θ represent the director, layer normal, and smectic tilt angle, respectively.

carried out under centrifugation and the reaction vessel then was cooled to room temperature. The polymeric liquid-crystal samples swollen with toluene were carefully removed from the vessel before the completion of the cross-linking reaction. These samples were simultaneously aligned by applying a uniaxial mechanical stress. First, a uniform director orientation was obtained by a uniaxial deformation. This sample had a uniform layer orientation and uniform director orientation in the Sm-A^* phase. In the Sm-C^* phase, however, smectic layers were conically distributed with the tilt angle θ of the layer normal to the mesogen long axis, where θ was identical to the tilt angle of the mesogenic groups in a smectic layer [Fig. 1 (left)]. We called this uniaxially deformed elastomer LCE1. To also obtain a uniform layer orientation, a second uniaxial stress was applied with an angle of $\varphi = 90^\circ - \theta$ to the first deformation direction. A biaxially deformed elastomer with uniform layer orientation as well as uniform director orientation was obtained by the second uniaxial stress [Fig. 1 (right)]. This elastomer was called LCE2. During the deformation process at room temperature, the toluene evaporated continuously from the samples and the samples underwent the processes from the isotropic phase of the gel to the tilted smectic phase of the dry elastomer [30]. The molecular alignments of these elastomers were confirmed by x-ray measurements [28]. The elastomer showed the following phase sequence: g − 6Sm-X^*32Sm-C^*80Sm-A^*115I(°C) (where g refers to the glassy state).

The transition temperatures listed above were determined by differential scanning calorimetry and x-ray scattering as already reported in previous papers [17,31]. The glass transition temperature was −6 °C. The Sm-X^* phase was a high-ordered tilted smectic phase.

Figure 2(a) shows the schematic of the experimental setup. The z axis was taken along the direction of the director in the LCE1, but along the layer normal in the LCE2 at room temperature. An electric field was applied parallel to the x axis, which was perpendicular to the LCE film. The sample film was mounted on a hot stage (HS1, Instec) for temperature regulation during measurements. Before each measurement, the sample was held for at least 30 min at the measurement temperature. The temperature was controlled within 0.1 °C. Conductive grease (Circuit Works) was thinly coated on both surfaces of the elastomer sheet with a sample size of several mm^2. The thickness of the grease layer was about 80 μm. The fluorescent beads (F8823, Molecular Probes) were homogeneously dispersed on the grease on the upper side. The movement of the fluorescent beads under an electric field was monitored with a CCD camera (QICAM, Qimaging) attached to a microscope (BX51, Olympus) to calculate the field-induced strain of the elastomer film. In this experiment, therefore, the fluorescent beads should follow the deformation of the elastomer when subjected to the electric field. If the thickness of the grease layer were smaller than the linear dimension of the area covered by the grease, the elastomer deformation would be faithfully captured with the beads for a uniform strain. We checked this by using an elastic tape with a thin grease layer partially coated on it [27]. The size of image was 320 × 240 μm^2 (1392 × 1040 pixels). In the images, ten fluorescent beads were selected and the positions of the beads were attained by an image analysis method. The accuracy of displacement was about 20 nm (0.1 pixel).

Next, the two-dimensional strain tensor was obtained by the least-squares method from the data on the y and z coordinates of ten beads at different locations [26,27]. Assuming spatially uniform deformation in the LCE, the two-dimensional displacement gradient $\mathbf{D}(t)$ was given by

$$\delta \mathbf{r}_i(t) = \delta \mathbf{r}_i(0) + \mathbf{D}(t)\delta \mathbf{r}_i(0), \tag{1}$$

with

$$\delta \mathbf{r}_i(t) = \mathbf{r}_i(t) - \mathbf{r}_G(t), \tag{2}$$

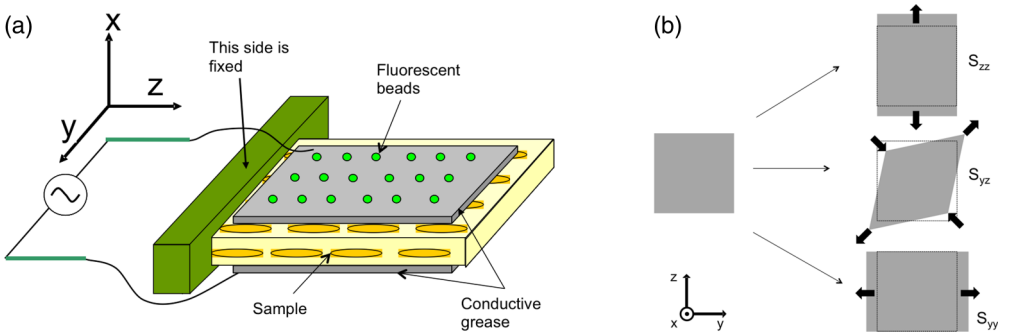

FIG. 2. (Color online) (a) Schematic of the experimental setup for this study. The left-hand side of the sample was fixed. The right-hand side could move freely, allowing small changes in the films to be precisely monitored. (b) Schematic for the measured deformations in the LCEs.

where $\mathbf{r}_i(t)$ is the position of the i bead at time t, $\mathbf{r}_G(t)$ is the center of mass for the measured beads, and $\delta\mathbf{r}_i(t)$ is the relative position of the ith bead from the center of mass. All the components of $\mathbf{D}(t)$ were determined by the least-squares method. Further, $\mathbf{D}(t)$ was decomposed into the pure strain tensor $\mathbf{S}(t)$:

$$\mathbf{S}(t) = \tfrac{1}{2}[\mathbf{D}(t) + \mathbf{D}(t)^T], \tag{3}$$

where superscript T indicated transpose. As reported in the previous study [26], we compared the $\delta\mathbf{r}_i(t)$ obtained from the experiment with the one calculated from the $\mathbf{D}(t)$ determined by the least-squares method. The $\delta\mathbf{r}_i(t)$ obtained from the experiment was in agreement with the value calculated from the obtained $\mathbf{D}(t)$, indicating that the assumption of uniform deformation was appropriate. Figure 2(b) shows the schematic for the measured deformations in the LCEs.

III. RESULTS AND DISCUSSION

The positions of ten beads were traced at 40 °C in the Sm-C^* phase during the application of a sinusoidal electric field. Figure 3 shows typical time courses of the displacement for one bead in both LCE1 and LCE2. Both the z and y components were clearly proportional to the applied electric field. Other traced beads in both LCE1 and LCE2 also showed the same sinusoidal behavior in the same phase, but with different amplitudes (note that the amplitudes can take a negative sign here). The displacements depended on the place of the beads on the elastomers, showing that strains related to these deformations were induced by the electric field. The directions of deformation in both elastomers also depended on the polarity of the applied electric field. These results indicate that spontaneous polarization was related to the deformation in both elastomers, not dielectric anisotropy as pointed out by Hiraoka *et al.* [12]. These behaviors seem to be the same as those reported previously on polydomain elastomer [12,26].

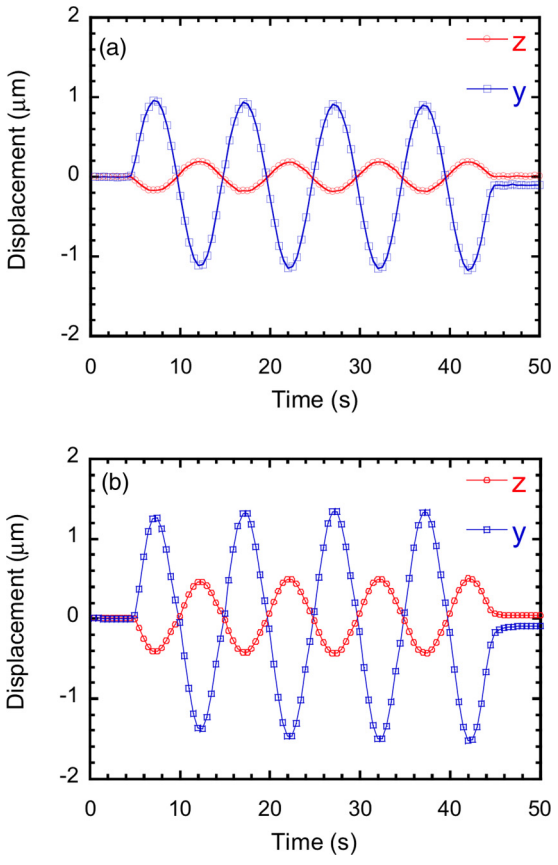

FIG. 3. (Color online) Time dependence of displacement of (a) LCE1 and (b) LCE2 at 40 °C. A sinusoidal electric field $E = E_0 \sin[2\pi f(t-5)]$ was applied with $f = 0.1$ Hz and $E_0 = 1.25\,\mathrm{V}/\mu\mathrm{m}$ during four cycles; E is zero at $t = 0{-}5$ and $45{-}50$ s.

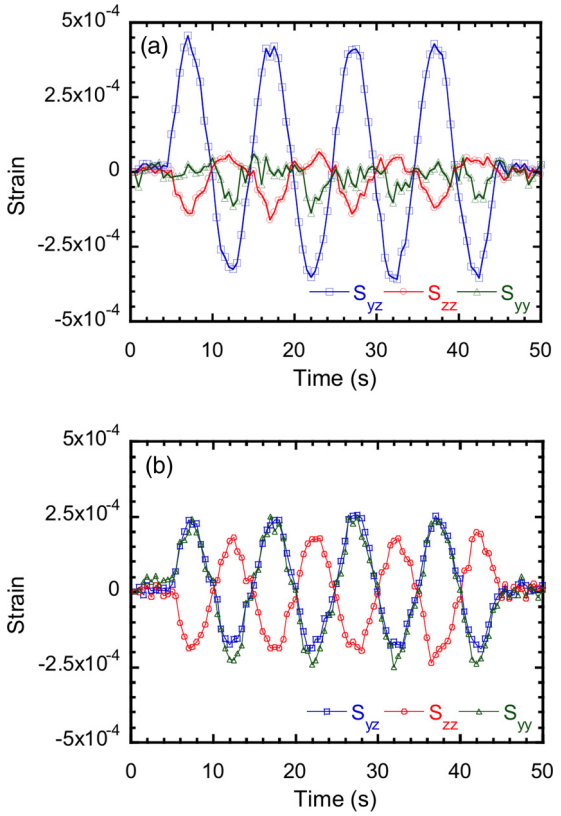

FIG. 4. (Color online) (a) Schematic for the measured deformation in the LCE. Also shown is the time dependence of strain tensors of (b) LCE1 and (c) LCE2 at 40 °C. The applied electric field is the same as in Fig. 3.

Although LCE1 and LCE2 behave similarly in displacement, their differences become apparent in the strain tensors. As shown in Fig. 4, the time dependence of the strain tensor $\mathbf{S}(t)$ is calculated from the displacements of the ten beads at different locations. In Fig. 4(a) of LCE1, the amplitude of S_{yz} is much larger than that of the others, meaning that the shear strain is mainly induced by the electric field. In contrast, the amplitudes of the three components of the strain are almost the same in LCE2, as shown in Fig. 4(b). This suggested that not only the shear deformation but also the elongation one along the y and z axes takes place in the LCE2 sample during the application of electric field. It is well known that the strain components depend on the frame of reference. Therefore, we will later discuss the results above in terms of the eigenvalues and eigenvectors of strain tensor.

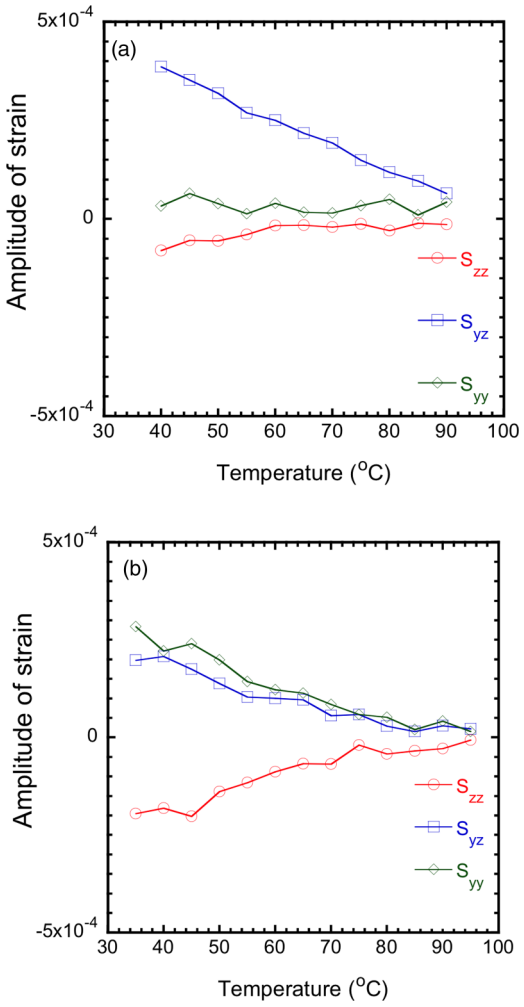

FIG. 5. (Color online) Dependence of the amplitude of strain tensors on temperature in (a) LCE1 and (b) LCE2. The applied electric field at each temperature is the same as in Fig. 3.

We obtained the amplitudes of the first harmonics of the strain tensors from the Fourier transform operation. Figure 5 shows the dependences of the amplitude of each strain tensor component on temperature in both LCEs. The negative values of amplitude mean that the strain and the electric field are mutually opposite in phase. For LCE1, S_{yz} clearly decreases with increasing temperature, but the other components are small and nearly constant. Meanwhile, all the components of LCE2 decrease with increasing temperature. It is reported that as the temperature increases in the Sm-C^* phase the tilt angle of the director decreases and then the spontaneous polarization also decreases. The decrease in the strain tensor components seems to be related to the decrease in the tilt angle (spontaneous polarization).

Here we develop a phenomenological consideration. Figure 6 represents the geometry of director $\mathbf{n}$ in the Sm-C^* phase. The order parameters inducing the Sm-A^*–Sm-C^* phase transition are $n_x n_z$ and $n_y n_z$ [32]. From symmetry considerations, we have approximate relations between the director and the strains

$$S_{xz} = c n_x n_z = c\theta\cos\phi, \quad S_{yz} = c n_y n_z = c\theta\sin\phi, \qquad (4)$$

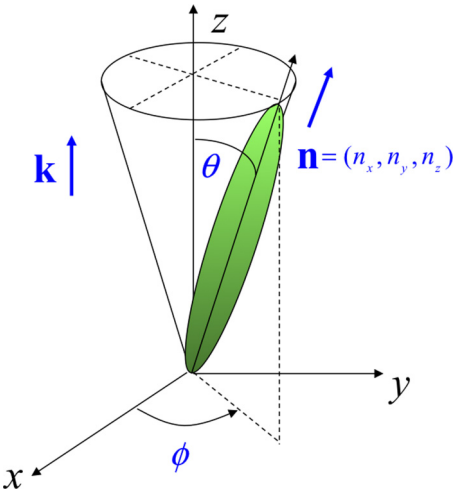

FIG. 6. (Color online) Typical schematic of a tilt angle of the liquid crystal in the Sm-C^* phase. Here ϕ is azimuthal angle in Sm-C^* phase.

with a constant c for a small tilt angle θ. Here ϕ is the azimuthal angle from the x axis. The other components of the strain tensor are of second order with respect to θ. Therefore, the shear strains are dominant. Note that this does not contradict the experimental result above that the shear and elongation deformations are comparable in the LCE2 sample because the strain components depend on the frame of reference, indicating that the LCE2 sample should be rotated as shown later. We assume that the electric field $\mathbf{E}$ is applied along the x direction. The field-induced parts of strains $\delta\theta$ and $\delta\phi$ can be written as $\delta\theta = \chi_\theta f_\theta$ and $\delta\phi = \chi_\phi f_\phi$, respectively, by using the susceptibility for the soft (amplitude) mode χ_θ and that for the phase mode χ_ϕ, where f_θ and f_ϕ are the forces conjugated to θ and ϕ, respectively. Assuming that $\theta = \theta_0$ and $\phi = \phi_0$ are at an equilibrium state without an electric field in Sm-C^*, the field-induced strains are given by

$$\begin{aligned} S_{xz} &= c\cos\phi_0\delta\theta - c\theta_0\sin\phi_0\delta\phi \\ &= -\tfrac{1}{2}c\mu\sin 2\phi_0\left(\chi_\theta - \chi_\phi\theta_0^2\right)E \end{aligned} \qquad (5a)$$

and

$$\begin{aligned} S_{yz} &= c\sin\phi_0\delta\theta + c\theta_0\cos\phi_0\delta\phi \\ &= -c\mu\left(\chi_\theta\sin^2\phi_0 + \chi_\phi\theta_0^2\cos^2\phi_0\right)E, \end{aligned} \qquad (5b)$$

where we use $\delta\theta = -\mu\chi_\theta E\sin\phi_0$ and $\delta\phi = -\mu\chi_\phi E\theta_0\cos\phi_0$ and μ is a constant, the sign of which depends on the sense of chirality [32]. Note that S_{yz} is observed in the present experiment, but S_{xz} could not be observed. It can be considered that for the LCE1 sample ϕ_0 is not constant and distributed from 0 to 2π, while in the LCE2 sample $\phi_0 \sim \pi/2$. From Eq. (5a), S_{xz} for the LCE1 sample may vanish by averaging over all the domains with different orientations, while that for the LCE2 sample may also be small due to large portions of domains with $\phi_0 \sim \pi/2$. Next, let us consider S_{yz}. As the sign of S_{yz} is independent of ϕ_0, each domain of the LCE1 sample contributes to S_{yz} in an additive manner. Generally, χ_θ is finite and increases as the transition point is approached, but χ_ϕ is thought not to have a strong temperature dependence.

Equation (5b) shows that the contribution of the amplitude mode to S_{yz} increases as the transition point is approached, while the contribution of the phase mode may decrease because the tilt angle decreases. The latter coincides with the experimental results in Fig. 5(a). Therefore, it can be concluded that the contribution of the phase mode primarily causes the electrically induced deformation whose magnitude increases with decreasing temperature in LCE1. Also in LCE2, the phase mode is thought to be dominant from the fact that the amplitudes of the three strain components increase similarly with decreasing temperature [see Fig. 5(b)]. For the ideal LCE2 sample with $\phi_0 = \pi/2$, S_{xz} and S_{yz} should disappear in the Sm-C^* phase.

To elucidate the essential differences between LCE1 and LCE2, we calculated the eigenvalues of the two-dimensional strain tensors at each temperature. The absolute values of eigenvalues in both LCEs decreased with the increase of temperature [Fig. 7(a)], which clearly indicates that the phase mode is responsible for the piezoelectric effect. Note that the sum of the two eigenvalues for each sample was almost zero, meaning that the area should be constant. The eigenvalues of the LCE2 were smaller than those of the LCE1 in magnitude. This can be explained by the above-mentioned distribution of ϕ_0. In the LCE1 sample, there was a certain number of domains with $\phi_0 \neq \pi/2$ contributing to the shear strain, while in the LCE2 sample, there was a comparably small number of such domains.

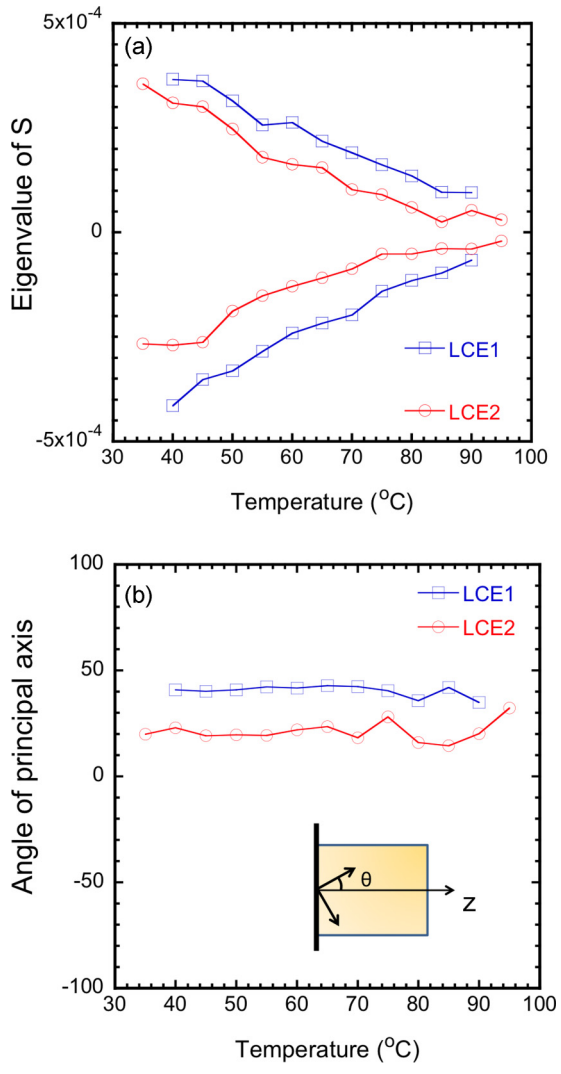

FIG. 7. (Color online) Temperature dependence of (a) eigenvalues and (b) the angle between one of the principal axes and the z axis in LCE1 and LCE2.

Figure 7(b) shows the temperature dependence of an angle between one principal axis and the z axis for each sample, which was obtained from the eigenvectors of the two-dimensional strain tensors. The result in Fig. 7(b) shows that the angles were almost independent of temperature for both samples. The angle was $40.4 \pm 2.6^\circ$ for LCE1 and $20.3 \pm 3.7^\circ$ for LCE2. In the case of the LCE1 sample, it can be said that the angle between the eigenvector and the z axis was approximately 45°, suggesting that the elongational strains along the z and y axes disappeared and the shear strain became dominant [Fig. 5(a)]. On the other hand, in LCE2 the angle was about 20°, which explains the appearance of the elongational strains in Fig. 5(b). It can be easily shown that the rotation of the y and z axes around the x axis change the temperature dependence of the strain tensor in Fig. 5(b) into that in Fig. 5(a), though the absolute values are different. The x-ray analysis shows that the angle between the director and layer normal is kept constant in LCE2 in the temperature range of the Sm-C^* phase, where the sample shape is almost unchanged [28]. This result is consistent with that in Fig. 7(b).

IV. CONCLUSION

We compared the piezoelectric properties of the two Sm-C^* elastomers with different domain structures. Direct observation of fluorescent beads dispersed on the sample enabled us to clearly measure the electrically induced deformation in both LCE1 and LCE2. The two samples showed different behaviors in strain tensor. The amplitude of the shear strain was larger than that of the elongation strain in LCE1, but all the components were almost the same in LCE2. The apparent difference was found to be due to the rotation of the principal axes in LCE2. On the other hand, it turned out that the absolute strain of LCE2 was smaller than that of LCE1 after calculating the eigenvalues of strain tensors, which was explained by the ϕ_0 dependence of the averaged piezoelectric constant.

ACKNOWLEDGMENTS

The authors thank Professor Tomoyuki Nagaya for valuable discussions. K.H. thanks Professor Heino Finkelmann for his encouragement. This paper was partially supported by the Hannam University Research Fund. This work was supported by Grant-in-Aids for Scientific Research on Innovative Areas "Fluctuation & Structure" (Grant No. 25103006) and for Scientific Research (B) (Grant No. 26289032) from the Ministry of Education, Culture, Sports, Science and Technology of Japan.

[1] P.-G. de Gennes, Phys. Lett. A **28**, 725 (1969).
[2] M. Warner and E. M. Terentjev, *Liquid Crystal Elastomers*, 2nd ed. (Clarendon, Oxford, 2007).
[3] E. Nishikawa, H. Finkelmann, and H. R. Brand, Macromol. Rapid Commun. **18**, 65 (1997).
[4] D. L. Thomsen, P. Keller, J. Naciri, R. Pink, H. Jeon, D. Shenoy, and B. R. Ratna, Macromolecules **34**, 5868 (2001).
[5] H. Finkelmann, E. Nishikawa, G. G. Pereira, and M. Warner, Phys. Rev. Lett. **87**, 015501 (2001).
[6] Y. Yu, M. Nakano, and T. Ikeda, Nature (London) **425**, 145 (2003).
[7] M. Camacho-Lopez, H. Finkelmann, P. Palffy-Muhoray, and M. Shelley, Nat. Mater. **3**, 307 (2004).
[8] J. Harden, M. Chambers, R. Verduzco, P. Luchette, J. T. Gleeson, S. Sprunt, and A. Jakli, Appl. Phys. Lett. **96**, 102907 (2010).
[9] R. Kohler, R. Stannarius, C. Tolksdorf, and R. Zentel, Appl. Phys. A **80**, 381 (2005).
[10] W. Lehmann, H. Skulpin, C. Tolksdorf, E. Gebhard, R. Zentel, P. Kruger, M. Losche, and F. Kremer, Nature (London) **410**, 447 (2001).
[11] C. M. Spillmann, B. R. Ratna, and J. Naciri, Appl. Phys. Lett. **90**, 021911 (2007).
[12] K. Hiraoka, M. Kobayasi, R. Kazama, and H. Finkelmann, Macromolecules **42**, 5600 (2009).
[13] R. B. Meyer, L. Liebert, L. Strzelecki, and P. Keller, J. Phys. Lett. (Paris) **36**, 69 (1975).
[14] O. Stenull and T. C. Lubensky, Phys. Rev. Lett. **94**, 018304 (2005).
[15] J. M. Adams and M. Warner, Phys. Rev. E **73**, 031706 (2006).
[16] J. M. Adams and M. Warner, Phys. Rev. E **79**, 061704 (2009).
[17] K. Hiraoka and H. Finkelmann, Macromol. Rapid Commun. **22**, 456 (2001).
[18] P. Heinze and H. Finkelmann, Macromolecules **43**, 6655 (2010).
[19] P. Papadopoulos, P. Heinze, H. Finkelmann, and F. Kremer, Macromolecules **43**, 6666 (2010).
[20] T. Eckert, H. Finkelmann, M. Keck, W. Lehmann, and F. Kremer, Macromol. Rapid Commun. **17**, 767 (1996).
[21] W. Lehmann, P. Gattinger, M. Keck, F. Kremer, P. Stein, T. Eckert, and H. Finkelmann, Ferroelectrics **208-209**, 373 (1998).
[22] F. Kremer, W. Lehmann, H. Skupin, L. Hartmann, P. Stein, and H. Finkelmann, Polym. Adv. Technol. **9**, 672 (1998).
[23] W. Lehmann, N. Leister, L. Hartmann, D. Geschke, F. Kremer, P. Stein, and H. Finkelmann, Mol. Cryst. Liq. Cryst. **328**, 437 (1999).
[24] W. Lehmann, L. Hartmann, F. Kremer, P. Stein, H. Finkelmann, H. Kruth, and S. J. Diele, Appl. Phys. **86**, 1647 (1999).
[25] K. Hiraoka, P. Stein, and H. Finkelmann, Macromol. Chem. Phys. **205**, 48 (2004).
[26] Y. H. Na, Y. Aburaya, H. Orihara, and K. Hiraoka, Phys. Rev. E **83**, 061709 (2011).
[27] Y. Aburaya, Y. H. Na, H. Orihara, and K. Hiraoka, Korea-Aust. Rheol. J. **24**, 83 (2012).
[28] K. Hiraoka and K. Mochida, Liq. Cryst. **40**, 669 (2013).
[29] H. Finkelmann, H. J. Kock, and G. Rehage, Macromol. Chem. Rapid Commun. **2**, 317 (1981).
[30] K. Hiraoka, N. Tagawa, and K. Baba, Macromol. Chem. Phys. **209**, 298 (2008).
[31] K. Hiraoka, W. Sagano, T. Nose, and H. Finkelmann, Macromolecules **38**, 7352 (2005).
[32] I. Musevic, R. Blinc, and B. Zeks, *The Physics of Ferroelectric and Antiferroelectric Liquid Crystals* (World Scientific, Singapore, 2000).